Impeller Characterization and Selection: Balancing Efficient Hydrodynamics with Process Mixing Requirements

Márcio B. Machado
Dept. of Chemical and Materials Engineering, University of Alberta, Edmonton, Alberta, Canada, T6G 2G6

José Roberto Nunhez
School of Chemical Engineering, State University of Campinas, UNICAMP, Campinas, SP, Brazil

David Nobes
Dept. of Mechanical Engineering, University of Alberta, Edmonton, Alberta, Canada, T6G 2G8

Suzanne M. Kresta
Dept. of Chemical and Materials Engineering, University of Alberta, Edmonton, Alberta, Canada, T6G 2G6

DOI 10.1002/aic.12758
Published online October 21, 2011 in Wiley Online Library (wileyonlinelibrary.com).

Current literature relies almost exclusively on the power number to compare and characterize impellers. Industrial mixing requirements may rely on conditions far away from the impeller. A protocol is proposed to compare impellers designed for turbulent mixing on the basis of impeller hydrodynamic performance and mixing process objectives. A hydrofoil impeller (KPC), and a mixed-flow impeller (45° down-pumping PBT), each at two diameters, were used to test the protocol. Fourteen measures were considered. Five are recommended for full characterization: power number, momentum number, and peak rate of dissipation of turbulent kinetic energy to characterize conditions at the impeller; power at just-suspended speed to compare the efficiency of solids suspension at the bottom of the tank; and point of air entrainment as a measure of turbulence penetration to the free surface. These five measures provide complete information about mixing performance and good differentiation between the impellers and geometries. © 2011 American Institute of Chemical Engineers *AIChE J,* 58: 2573–2588, 2012
Keywords: mixing, impeller performance, power number, momentum number, micromixing

Introduction

The bulk of the mixing literature compares impellers based on a single-performance criterion, but when considering a new impeller it would be useful to have a defined subset of characteristics which covers the range of impeller performance and process requirements in stirred tanks and provides a standard basis for comparison. In this article, 14 measurements are considered for inclusion on this list. They fall into one of two categories: hydrodynamic characteristics of the impeller or mixing performance characterization in different regions of the tank.

The six hydrodynamic characteristics include:

- The power number (N_p).
- The flow number (N_Q).
- The momentum number (Mo).
- The intensity of turbulence as characterized by either the average power dissipated per unit mass ($P/\rho V_{\text{tank}}$), the power dissipated per unit mass in the impeller swept volume ($P/\rho V_{\text{swept}}$), or the dimensionless local rate of dissipation of turbulent kinetic energy ($\varepsilon_{\max}/N^3D^2$).

The eight mixing performance characteristics focus on different parts of the tank and include:

- Impeller speed required for off-bottom solids suspension (N_{js}).
- Power consumption at N_{js} (P_{js}).
- The Zwietering constant (S).
- Impeller speed required for entrainment of air into the liquid at the free surface (N_E).
- Power consumption at N_E (P_E).
- Micromixing efficiency as measured by the yield of desired product in three locations: at the impeller (Y_I), at the surface (Y_S), and close to the baffles (Y_B).

In the following, the significance of these measures is discussed and why they were selected as candidates for a comparison protocol.

Hydrodynamic characteristics

Classical methods of impeller characterization were adapted from the literature on pumps and focus on hydrodynamic characteristics.[1] Two of these tests are based on angular and axial momentum balances around the impeller. An angular momentum balance gives the torque on the shaft and the power consumption, or shaft work, leading to N_P. An axial momentum balance can be used to find the axial thrust on the shaft due to acceleration of the fluid, giving Mo. The bulk circulation, or macromixing, is partially characterized by the volumetric flow rate leaving the impeller (N_Q) and the micromixing is characterized by some measure of turbulence intensity. The first measure of turbulence intensity in the literature was derived from

Correspondence concerning this article should be addressed to M. B. Machado at marcio@ualberta.ca.

an overall energy balance on the tank. Conservation of energy requires that the power entering through the shaft is dissipated by viscous dissipation in turbulent eddies. This gives the average power dissipated per unit mass in the tank ($P/\rho V_{tank}$). Once it was shown that the impeller interacts with the tank walls and that the turbulence varies dramatically over the tank volume, this integral measure was modified to obtain a more accurate scaling variable: the total power input per unit mass in the impeller swept volume ($P/\rho V_{swept}$). Since no attempt is made to estimate what percentage of the power is actually dissipated in the impeller swept volume, this second measure is not an absolute measure of the turbulence. The local rate of dissipation of turbulent kinetic energy (ε) is a direct measure of local turbulence intensity. Some preliminary ranking of these variables can be accomplished from considering their theoretical basis and their application to mixing problems in current literature.

The *power number* N_p, is based on an angular momentum balance around the impeller[1–3,71] and is one of the most widely used design specifications in mixing operations

$$N_P = \frac{P}{\rho N^3 D^5} \tag{1}$$

The power number is a function of the Reynolds number and geometry of the system, including all dimensions of the impeller and the position(s) of the impeller(s) in the tank,[4,5] but the most significant variable is the geometry of the impeller.[1,6] For fully turbulent flow of a single-phase fluid, N_p is a constant. The fully turbulent N_p is considered the most important hydrodynamic characteristic of an impeller.

Power number data taken for a single impeller can only be extended to more complex geometries under certain limited conditions. For a double PBT configuration, Armenante[5] determined that the power draw is smaller than twice the power draw of a single impeller. Fujasová[7] and Nocentini[8] concluded that adjacent impellers do not interfere when the distance between them is more than double that of their diameter, and in this case their combined power number is equal to the sum of power numbers measured in the single-impeller configuration.

No impeller characterization would be complete without N_p and this is well established in the literature, so it is included in the protocol as the base measurement. Once the power number is determined, the power consumed per mass of the fluid in the tank can be estimated. The power per mass ($P/\rho V_{tank}$ or $P/\rho V_{swept}$) has proven to be a reliable predictor of a number of process results,[2,6] and it is also a very common criterion used to scale-up mixing tanks.[9]

The *pumping number,* or *flow number* N_Q, is a measure of the flow leaving an impeller and was widely cited in the literature for a number of years.[10–20] Considering a cylindrical control volume around an impeller, the discharge surface of a down pumping axial impeller is the lower surface and the normal component is the axial velocity. For purely axial impellers the normal (radial) velocity at the tip of the blades provides a very small contribution to the flow number and is often neglected. This gives the flow number for axial impellers

$$N_Q = \frac{\int_0^R 2\pi V_z r dr}{ND^3} \tag{2}$$

For radial impellers, the integral of the radial velocity component over the tips of the blades is the most important term. The radial jet leaving the impeller entrains fluid as it moves out into the tank, so by the time the jet reaches the baffles $Q_{jet} = 3^* Q_{imp}$ for $D = T/4$.[21] For mixed flow impellers, both the tip of the blades and the lower surface of the impeller contribute to the flow. The flow number is included for reasons of historical completeness, but the flow number has not been successfully used in a design correlation to date.

The momentum number *Mo*, is a relatively new concept which has been introduced by several authors.[22–24] Bhole[23] compared two axial flow impellers for pulp fiber suspensions in the laminar and transitional regimes, where both the power number and axial thrust number (similar to *Mo*) are functions of the Reynolds number. Jones[24] used the ratio of the inlet pipe momentum to the impeller discharge momentum to balance the flow and eliminate short circuiting in a CSTR. Grenville[22] successfully compared blend times in a jet mixed vessel and an impeller mixed vessel in terms of momentum.

The *momentum number Mo*, arises from an axial momentum balance around the impeller. While the angular momentum balance relates the increase in angular momentum to the torque on the shaft and the power number, the axial momentum balance relates the increase in axial momentum of the fluid to the thrust, or upward force on the shaft and the motor. The axial momentum is also convenient because it is a conserved quantity.[21] Unlike the volumetric flow, which changes, the momentum stays constant as the impeller discharge flow entrains the surrounding fluid and moves downward (or radially outward) in the tank.[25] The axial momentum balance is given by the integral over a cylindrical control volume surrounding the impeller

$$F_z = \int_A \rho \vec{V} \bullet \vec{n} V_z dA \tag{3}$$

To compare thrust between axial impellers, the net axial momentum added to the flow between the upper and lower surfaces would be considered, but the total axial momentum leaving the impeller is of more interest for correlating process objectives. In dimensionless form, this is given by

$$Mo = \frac{\int_0^{D/2} \rho V_z^2 2\pi r dr}{\rho N^2 D^4} \tag{4}$$

No definition of *Mo* is proposed for radial impellers since they are not designed to generate axial momentum.

Brown[26] observed that the momentum number is proportional to the flow number squared ($Mo \propto N_Q^2$) for a wide range of experimental data. Applying this observation to Eq. 4 gives

$$\frac{\int_0^{D/2} 2\pi r V_z^2 dr}{N^2 D^4} \propto \left(\frac{\int_0^{D/2} 2\pi V_z r dr}{ND^3} \right)^2 \tag{5}$$

For most axial and mixed flow impellers, the axial velocity profile can be approximated by 2-3 straight lines. Considering the simplest case of a single straight line with $V_z = br$ gives

$$\frac{2\pi}{N^2 D^4} \int_0^{D/2} r(br)^2 dr \propto \frac{4\pi^2}{N^2 D^6} \left(\int_0^{D/2} r b r dr \right)^2 \tag{6}$$

After integrating and applying the limits, the slope of the velocity profile segment, b, drops out

$$\frac{(D/2)^4}{4} \propto \frac{2\pi}{D^2}\left(\frac{(D/2)^3}{3}\right)^2 \tag{7}$$

which gives the constant of proportionality

$$Mo = \frac{9}{2\pi}N_Q^2 = 1.43N_Q^2 \tag{8}$$

For the same relationship, Brown[26] presented an experimental constant of 1.46 with a correlation coefficient of 0.99 over a range of scales and impeller geometries.

The momentum number was selected as a promising alternative to the flow number. The slightly different physical meaning has already proven to be more successful than the flow number for correlating macromixing phenomena such as the blend time,[22,26] and the derivation above suggests that historical data for N_Q may be easily converted to *Mo*.

While N_p gives the power draw of an impeller and *Mo* gives an indication of bulk flow, both of these are integral, or averaged, quantities. A range of scales of motion coexist in a stirred tank: the mean flow (or global circulation), the periodic fluctuations (or trailing vortices) induced by the blade passages in the impeller region, and the random fluctuations at the smallest scales that finally dissipate the kinetic energy.[27] The turbulence parameters of most direct relevance to impeller performance are the characteristic length scales of turbulence and the *local rate of dissipation of turbulent kinetic energy* (ε),[28] which determines the local turbulence intensity and degree of micromixing. The local rate of dissipation of turbulence kinetic energy is a key parameter in stirred tanks and its local value has a strong influence on the performance of many mixing processes.[29] Both the maximum dissipation and the distribution of energy over the tank influence bubble, drop and particle breakdown, mass transfer, and apparent reaction rates.[30]

Direct measurement of the local dissipation rate by experiments is difficult because the derivatives of the smallest turbulent structures must be captured.[31] Several methods for estimating the energy dissipation rate have been proposed.[32] Cutter[33] developed an equation relating ε to the three components of mean and fluctuating velocities. Okamoto[34] integrated a one-dimensional (1-D) energy spectrum to estimate $\varepsilon = A\frac{q^{3/2}}{L_{res}}$. Wu[28] used the expression to estimate the local dissipation, where A is a constant (≈ 1 for locally isotropic turbulence), q is the turbulent kinetic energy, and L_{res} is a 3-D resultant macrolength scale. Kresta[32] showed that a simple 1-D estimate can be used close to the impeller

$$\varepsilon = A\frac{u'^3}{L} \tag{9}$$

where u' is the rms of the fluctuating velocity component in the dominant flow direction, and L is the integral-length scale of turbulence. Kresta[32] also showed that L is equal to the size of the trailing vortices ($L = D/10$) close to a PBT and Zhow[35] extended this result for the Rushton and A310 impellers. Close to the impeller, this estimation gives results which are within $\pm 30\%$ of the more rigorous measurement methods.[32] In the bulk of the tank, the assumptions needed to justify the estimate are not valid and the full detailed measurement methods must be used.[27,36] Zhou[35] compared the energy distribution between convective and turbulent flow in the impeller discharge stream for three frequently used impellers: the Rushton turbine, PBT and A310. The A310 is most efficient at generating convective flow (macromixing), the Rushton generates the most turbulence (micromixing), and the PBT recovers the most energy from the return flow.

Recent articles report direct measurements of the dissipation rate. Baldi[37] used PIV and LDA techniques to measure the turbulence energy dissipation rate in vessels stirred by Rushton impellers. The fluctuating gradient results obtained with the two techniques showed good agreement and suggest that direct measurement of the ε distribution is now feasible with both PIV and LDA methods. Ducci[36] assessed different ways of calculating ε from direct measurements and from dimensional relations. The authors concluded that under similar assumptions of statistical isotropy, the agreement found between the two techniques was good (10–30% difference), but that dimensional methods which assume isotropic flows under anisotropic conditions may underestimate the dissipation rate maximum by up to 40%. Roussinova[38] found a similar error when the isotropic assumption was applied under conditions where large macroinstabilities were present in the flow. The stirred tank is a complex recirculating flow, and rigorous and robust measurements of the local dissipation require careful thought and often 10 years of work. The literature suggests, however, that an initial comparison between impellers can be achieved relatively quickly from Eq. 9. Realizing that the uncertainty on the more exacting methods is still $\pm 20\%$, we find that the estimate of ε given by Eq. 9 is a reasonable way to proceed for an initial impeller characterization, providing the uncertainty in the measurement is retained in the reporting and the measurements are made close to the impeller. This equation was selected for inclusion in the protocol.

In the absence of fluctuating velocity measurements and a direct measure of local dissipation, several average measures of dissipation were selected as possible alternatives. The first is the *power per unit mass over the tank volume* $P/\rho V_{tank}$. This measure gives the average dissipation over the whole tank volume but can only be applied in the case of exact geometric similarity. It also dramatically distorts the level of dissipation,[6] since values close to the impeller are known to be approximately 100 times the values in the bulk of the tank for the Rushton turbine.[25] A more accurate estimate is the *power per unit mass over the impeller swept volume* $P/\rho V_{swept}$. This measure implicitly assumes that all of the energy is dissipated in the impeller swept volume. The fraction actually dissipated in the impeller swept volume is of the order of 30–50%[35,39] and is a function of the impeller geometry. The advantage of using the swept volume is that it takes the effect of impeller diameter into account for scale-up and comparison of impeller configurations. Both of these measures are frequently used for both scale-up and experimental design when measures of local dissipation are not available.

The five hydrodynamic measures considered for the protocol are obtained from torque and velocity measurements. The power number provides the base characteristic of the impeller and requires accurate measurement of the torque on the shaft under fully turbulent conditions. If profiles of the mean and fluctuating velocities in the impeller discharge stream are available, the momentum number and the local dissipation can be calculated. Both of these characteristics have been successfully used in a number of correlations. Where velocity measurements are not available, two estimates of average dissipation have been proposed: the power dissipated per unit mass in the tank, and the power dissipated per unit mass in the impeller swept volume.

Mixing performance measures

There are three scales of mixing in a stirred tank: macromixing, mesomixing and micromixing.[6,40] Macromixing is a

function of the largest scales of motion in the fluid and micromixing is function of the smallest scales of motion and the final scales of molecular diffusivity (Kolmogorov and Batchelor scale, respectively). Mesomixing is a scale of mixing smaller than bulk circulation but larger than micromixing scales[41] where turbulent diffusivity and inertial convection are important.[42] Mesomixing is particularly important at the feed point[43–45] and it may influence the micromixing performance.[46] A better understanding of mesomixing would be very useful but at present there is no well established method for characterizing mesomixing performance in the literature. For this reason, mesomixing was not included in the protocol.

The mixing performance measures selected consider mixing conditions at different locations in the tank over a range of mixing scales from macromixing to micromixing. Blend time is a clear measure of macromixing performance in turbulent flow, but it is very well correlated with the power number,[47] so no additional information is gained from its measurement and it was not included. Conditions at the bottom of the tank were compared using solids suspension, which is affected by particle properties, mean flow, and local turbulence. Conditions at the surface of the fluid were characterized using both the point of air entrainment and the micromixing performance for surface feed, both dominated by local turbulence. Micromixing conditions at the impeller, at the surface, and close to the baffles were all included due to the importance of mixing for reactor design. No clear measure or indicator of mesomixing performance was identified.

Solid–liquid mixing in stirred tanks has a wide variety of industrial applications. There are two important operating requirements for these processes: complete off-bottom suspension and an even distribution of solids throughout the tank.[48,49] According to the Zwietering criterion,[50] complete off-bottom suspension occurs when no particles stay on the bottom of the tank for more than 1 or 2 s. This impeller speed is called *the just suspended speed* (N_{js}). If the solids concentration is less than 10 wt %, N_{js} can be estimated using the Zwietering correlation

$$\mathrm{N_{js}} = \mathrm{S_Z} \cdot \left(\frac{\mathrm{g}.(\rho_\mathrm{S} - \rho_\mathrm{L})}{\rho_\mathrm{L}} \right)^{0.45} \frac{\mathrm{X}^{0.13} \mathrm{d_p}^{0.2} \nu^{0.1}}{\mathrm{D}^{0.85}} \tag{10}$$

While Zwietering included the effect of impeller diameter in his correlation; later studies have shown that N_{js} also depends on the off-bottom clearance.[51–53] Because of this, the *Zwietering constant* (S_Z) is a characteristic of both the impeller geometry and the tank configuration. It is expected to be independent of the type of solids used.

The *power consumption at* N_{js} (P_{js}) is

$$\mathrm{P_{js}} = \mathrm{N_p} \rho_\mathrm{slurry} \mathrm{N_{js}^3 D^5} \tag{11}$$

Most of the literature on solids suspension focusses on determining S_Z for various geometries, and on defining the key variables for this process objective. A recent article by Ayranci[53] compares the power consumption of a range of geometries. The results show that P_{js} may be a better indicator of impeller performance than S_Z. Özcan-Taskin[54] came to the same conclusion for the draw-down of floating solids. All three characteristics were retained for comparison in this study.

The point of air entrainment N_E is the impeller speed at which air is first entrained from the surface of a stirred tank. The point of air entrainment holds potential as a characteristic for several applications. First, there is the twin purpose of either needing to avoid gas entrainment, or to draw gasses in from the head space. In the first case, a large N_E is desirable, in the second; a small N_E and P_E are desirable. Bhattacharya[55] showed that air entrainment at the liquid surface in a stirred tank is caused by interaction between the interfacial tension and the turbulent eddies at the surface. This characteristic makes N_E a useful characteristic for a second application: the scale-up of reactions with surface feed. Since the turbulent flow field at the surface of a stirred tank is a complex function of the rotational speed, the impeller geometry, the impeller position and the tank geometry, the point of air entrainment is difficult to correlate.[55] The characteristic N_E allows a comparison of the amount of turbulence at the surface between different impeller geometries and tank configurations. Both N_E and P_E were selected for consideration in the protocol.

Mixing at the scale of the smallest eddies or striations (*micromixing*) may influence selectivity, yield and quality of final products in many industrial processes such as polymerization and precipitation. Stirred tanks have highly nonuniform mixing conditions and require careful feed addition strategies for successful reactor design.[56] To improve the reactor performance, it is important to characterize the local micromixing.[57] In many cases multiple reactions producing both desired and undesired products can occur as parallel competing reactions. In these competing reactions, the reactant is consumed by two alternate reaction paths to form different products. The goal then is to minimize the formation of undesired products and maximize the yield of desired products. Previous mixing studies have shown that yields of desired products are maximized when the reactants are fed into a region of high turbulence in the tank, i.e., at the impeller suction using submerged feed pipes or dip-tubes. This is not always practical in industrial applications where process corrosivity, mechanical vibrations, backmixing (reactions occurring in the dip-tube due to low-feed rates), and plugged lines are all concerns.

The iodide-iodate parallel competitive reaction[57–62] was used to compare the micromixing efficiency of the impellers. The neutralization reaction forming the desired product, boric acid (H_3BO_3) is expressed as Eq. 12 and the slower, parallel redox reaction forming undesired products iodine and water as Eq. 13. The unwanted byproduct iodine from Eq. 13 reacts further to form triiodide ion as expressed in Eq. 14

$$\mathrm{H_2BO_3^-} + \mathrm{H^+} \Leftrightarrow \mathrm{H_3BO_3} \tag{12}$$

$$5\mathrm{I^-} + \mathrm{IO_3^-} + 6\mathrm{H^+} \Leftrightarrow 3\mathrm{I_2} + 3\mathrm{H_2O} \tag{13}$$

$$\mathrm{I_2} + \mathrm{I^-} \Leftrightarrow \mathrm{I_3^-} \tag{14}$$

The first reaction (Eq. 12) is much faster than the second.[58] Under perfect mixing conditions, all of the H^+ present in the system reacts in the first reaction. Otherwise, under imperfect mixing conditions, local high concentrations of H^+ can occur and the undesired products are formed. Bourne[63] studied the kinetics of this reaction and concluded that this method gives qualitatively consistent and intelligible results; however, the quantitative conclusions must be considered carefully.

Micromixing experiments have also been used as a way to measure ε indirectly[64] and they are known to perform well under some conditions. The question posed here is whether

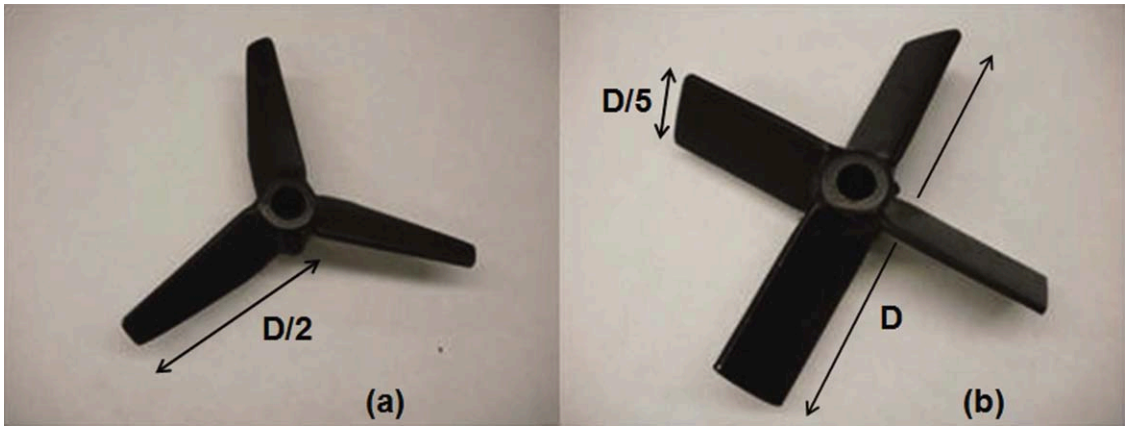

Figure 1. The KPC T/2 (a) and the 45° down-pumping pitched blade turbine T/2 (b) impellers used in the experiments.

this method is robust and generally applicable over the entire tank volume, and if so, which feed points should be selected. Conversely, micromixing experiments may be best reserved to characterize mixing performance for a specific set of reaction conditions[65] with more direct measures of local turbulence used to characterize the impeller performance and confirm the micromixing results.

Impeller selection criteria provide important information for the design of a stirred tank, particularly where a new impeller design is being considered. The objective of this work is to propose a protocol to compare impellers across the full range of mixing and hydrodynamic performance. Two impellers, the standard 45° down-pumping PBT and a relatively new KPC hydrofoil were selected to test a number of measures of mixing performance to select a subset of characteristics for inclusion in the protocol. The following measurements are considered:

- Power number N_P, a measure of relative power consumption
- Flow number N_Q, a measure of volumetric flow at the impeller discharge
- Momentum number *Mo*, a measure of axial momentum discharged by the impeller
- Maximum dissipation ε_{max}, $P/\rho V_{tank}$, or $P/\rho V_{swept}$, measures of turbulence intensity
- Just suspended speed N_{js}, the Zwietering constant S, and power consumption at just suspended speed P_{js}, which are measures of mixing conditions at the bottom of the tank
- Air entrainment speed N_E, and power at the point of air entrainment P_E, which give an indirect measure of turbulence levels at the liquid surface
- Micromixing efficiency, which is a key parameter for reactor design, and gives a measure of turbulence levels at the feed point. Three feed points are identified, with three corresponding yields (Y_S, Y_B, Y_I).

The selection of one impeller over another depends on the mixing requirements of the process.[66] This protocol is designed to provide information which encompasses a representative range of criteria so that engineers can more efficiently select a suitable impeller and tank configuration based on the varying process needs encountered in new mixing applications.

Experimental

The two impellers shown in Figure 1 were used for testing and refinement of the protocol (a) a three bladed KPC hydrofoil impeller, and (b) a four-bladed down-pumping 45° pitched blade turbine (PBT). The PBT was chosen as the base case since it is well characterized and common in industry. The PBT is a mixed flow impeller with both radial and axial flow components in the discharge stream. As the fluid viscosity increases, the discharge flow becomes more radial. The Kroma KPC impeller is a high-efficiency hydrofoil.[67] Hydrofoils have nearly constant pitch across the blade length, so the resulting uniform velocity profile gives a lower power number and higher energy efficiency for flow generation than the pitched blade turbine[9] or the Rushton turbine. These impellers are used for applications where purely axial discharge flow is important, and low shear and/or power are desired.

The experiments were carried out in the ($T = 0.240$ m) diameter cylindrical flat-bottom tank illustrated in Figure 2. Four rectangular baffles with a width of $w_b = T/10$ were equally spaced around the periphery of the tank. Two impeller diameters ($D = T/3 = 80$ mm, and $D = T/2 = 120$ mm) were used with the dimensions given in Table 3. Both PBT impellers had the same blade width ($w = D/5$). The off-bottom clearance (C) of the impeller, measured to the bottom of the blades, and the impeller submergence below the surface

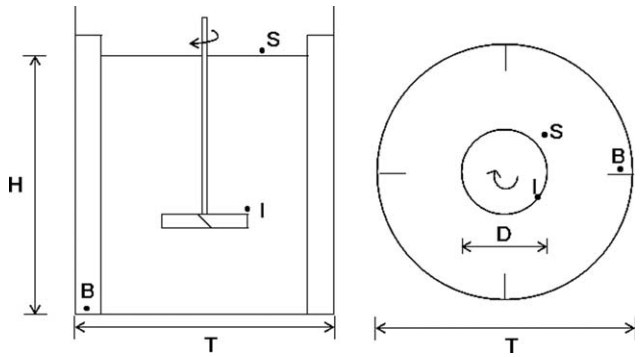

Figure 2. Feed locations in the micromixing experiments: S is 2 mm above the liquid surface and 50 mm from the shaft; I is 5 mm above the impeller suction at the blade tip and at *r* = 60 mm for T/2 impellers; r = 45 mm for T/3 impellers; B is in front of the baffle, 5 mm from the bottom of the tank, 2 mm from the wall and 2 mm from the baffle.

(S), measured to the top of the blades, was varied. The test fluid was water and the liquid depth H, was set equal to the tank diameter ($H = T$) for all experiments.

Power number (N_P)

The power number was measured according to the method described by Chapple.[2] The Reynolds number ($Re = ND^2/v$) was varied over the full practical range: from 2.4×10^4 to 9.6×10^4 for the $D = T/2$ impeller, and from 1×10^4 to 4.2×10^4 for the $D = T/3$ impeller. Below the lower limit the torque was too small to measure accurately and above the upper limit the vibrations were too severe for safe operation. The impellers were located at an off-bottom clearance of $C = T/3$ for all Reynolds numbers. Selected power numbers were also measured at Reynolds numbers of 32 000 and 48 000 and $C = T/4$ to complement the pumping and momentum number data.

Flow number (N_Q) and momentum number (Mo)

The flow number and the momentum number were calculated from the time and angle averaged axial velocity profile 3 mm below the impeller, according to Eqs. 2 and 4. The four impellers were placed at two different off-bottom clearances, $C = T/3$ and $C = T/4$. Measurements were carried out in the fully turbulent flow regime ($Re = 32\,000$ and $Re = 48\,000$).

The velocity was measured using a stereoscopic PIV system. The cylindrical tank was placed inside a transparent square tank filled with water to minimize refraction at the cylindrical surface of the inner vessel. Two high-resolution cameras (LaVision, Imager Pro X, 14 bits, 2048 × 2048 pixels) captured images of a seeded flow field which was illuminated with the double pulse of an Nd:YAG laser (Spectra Physics, PIV-400, 532 nm, 10 Hz, 400 mJ of energy per pulse). The seeding particles were hollow glass beads with a mean diameter of 11 μm (Potters Industries) and a specific gravity of 1.1. The cameras were positioned underneath the square tank. The system was calibrated using a calibration plate 3 mm below the impeller. The cameras were positioned to take pictures of at least one third of the KPC impeller discharge area and one quarter of the PBT impeller discharge area. Regions affected by the shadows cast by the impellers and baffles were excluded from the analysis.

For each operating condition, 1000 image pairs were recorded with a time interval between the two images of 200–450 μs. The time interval was adjusted to obtain an average particle displacement of 10 pixels. A 3-D cross-correlation algorithm was used to determine particle displacement between the two images. Velocity vectors were calculated using a commercial software package (LaVision, Davis 7.4) with interrogation cell sizes of 64 pixels for the preliminary step, and 32 pixels with 50% overlap for the final step. The resulting data gives three components of instantaneous velocity over the measurement plane. The frequency of collection of image pairs was 1.6–2.5 Hz with 1000 images collected per data set. From each data set, the time and angle averaged mean and fluctuating velocity profiles were calculated for each velocity component and each impeller.

The mean axial velocity was used to calculate pumping and momentum numbers. Since PBT has four blades, only one quarter of its cross-sectional area was imaged. Since the KPC has only three blades, only one third of the cross sectional area was used.

Rate of dissipation of turbulent kinetic energy (ε)

The rate of dissipation of turbulent kinetic energy (ε) was estimated from the axial fluctuating (rms) velocity component 3 mm below the impeller, using the data collected at $Re = 48\,000$, and a clearance of $C = T/3$. The dissipation was estimated using equation, where $A = 1$ and $L = D/10$. The reader is cautioned that this equation has only been validated for measurements very close to the impeller, and several assumptions in the development of the method are not likely to hold in the bulk of the tank.

Just suspended speed (N_{js}) and power at just suspended speed (P_{js})

The just suspended speed is determined visually by observing the bottom of the tank. The impeller speed was increased in steps of 3 rpm. After the system reached steady state (in 1 to 2 min), the bottom of the tank was observed for at least 30 s.[53] This was repeated until the Zwietering criterion was satisfied.

Since N_{js} is a function of both the mixing geometry and the solids suspension properties, two types of spherical particles were used to determine N_{js} and P_{js}: glass beads ($\rho_S = 2500$ kg/m^3 and $dp = 74$–125 μm), and bronze particles ($\rho_S = 8855$ kg/m^3 and $dp = 150$–297 μm), each at a solids loading of 3 wt % (giving $X_{\text{glass beads}} = 3.09\%$ and $X_{\text{bronze}} = 3.09\%$ in Eq. 10). The off-bottom clearance of each impeller was varied from $C = T/6$ to $C = T/4$. Full details of the experimental rig are given by Ayranci.[53] The repeatability of the experiment depended on the type of particle used. Ayranci[53] observed that the small glass beads are difficult to see, giving results that vary by up to 38% between observers, while the bronze test particles are darker and gave repeatability within 15% between two observers. For a single observer, the repeatability between 24 h replicates of the experiments is within ±3 rpm.

Air entrainment speed (N_E)

The bubble-density-scale described by Bhattacharya[55] was used to determine the point of air entrainment N_E. In this procedure, the tank is first filled with water and the impeller is positioned at the desired submergence. The submergence, which is the distance from the liquid surface to the top surface of the impeller is varied from $S = T/24$ to $S = T/2$. The impeller is started and the tank is allowed to equilibrate for a period of 2-3 min. The impeller speed is then increased until the liquid surface becomes more active and a few bubbles are entrained, but quickly escape. As the impeller speed increases, the number of entrained bubbles also increases. When the impeller speed reaches N_E, there is a marked increase in the bubble population in the tank. During these experiments, the liquid surface at N_E was turbulent but there was no splashing or formation of sprays. While this method has a component of subjectivity, the bubbles have a high index of refraction, which makes them easy to detect. The results taken by two observers differed by less than 5%.

Micromixing efficiency

Micromixing experiments were used to evaluate the effects of local turbulence and feed location on the yield of desired product using the competitive-parallel iodide-iodate reaction scheme. The three feed locations shown in Figure 2 were selected to reflect the varying local turbulence in different regions of the tank. Feed at the impeller (I) is the

Table 1. Micromixing Experimental Conditions for Reynolds Number and N_E Scaling

Reynolds number	Impeller, D	N (rpm)	Re	ε_{max} (W/kg)
Re = 20 000	PBT T/3	190	$2.0x10^4$	0.55
	KPC T/3	190	$2.0x10^4$	0.06
	PBT T/2	84	$2.0x10^4$	0.13
	KPC T/2	84	$2.0x10^4$	0.02
N_E: point of	PBT T/3	560	$6.0x10^4$	14.04
air entrainment	KPC T/3	650	$6.9x10^4$	2.22
	PBT T/2	245	$5.9x10^4$	3.22
	KPC T/2	385	$9.2x10^4$	2.37

Table 2. Micromixing Experimental Conditions at Two Levels of Power per Mass ($P/\rho V_{tank}$)

$P/\rho V_{tank}$ (W/kg)	Impeller, D	N (rpm)	$P/\rho V_{swept}$ (W/kg)	ε_{max} (W/kg)
0.139	PBT T/3	442	27.51	6.90
	KPC T/3	650	38.50	2.22
	PBT T/2	209	7.40	2.00
	KPC T/2	327	10.36	1.45
0.011	PBT T/3	190	2.18	0.55
	KPC T/3	280	3.05	0.18
	PBT T/2	90	0.59	0.16
	KPC T/2	141	0.82	0.12

recommended feed location for mixing sensitive reactions. Surface feed (*S*) is sometimes selected for operational reasons, even though it is known to give a lower yield. The third feed point (*B*) is placed in the bulk of the tank close to the baffle and is expected to give yields between the surface feed (Y_S), and the impeller feed (Y_I).

Full details of the micromixing experimental conditions are given in Tables 1 and 2. Three different scaling approaches were used to design the experiments:

- equal Reynolds number ($Re = 20\ 000$),
- equal surface turbulence based on the point of air entrainment (N_E), and
- equal power consumption ($P/\rho V_{tank}$).

Equal Reynolds number gives a direct comparison between impellers in terms of the flow regime and balance between inertial and viscous forces, but is not recommended as a scale-up or scale-down criterion. Bhattacharya[55] showed that at N_E, similar turbulence conditions exist at the surface, making it a good performance measure for surface feed. Equal power draw is the traditional method for scale-up and scale-down so two levels of power draw were selected: a low-power per mass ($P/\rho V_{tan\,k} = 0.011$ W/kg) and a high-power per mass ($P/\rho V_{tan\,k} = 0.139$ W/kg). Since $P/\rho V_{tank}$ does not scale the dissipation at the impeller correctly with changes in diameter,[25] the results are also considered in terms of the power per swept volume ($P/\rho V_{swept}$), and the maximum local energy dissipation at the impeller (ε_{max}).

In the experiment, a small amount of sulfuric acid is added to a mixture of iodate, iodide and borate ions. In perfect mixing conditions, the injected acid is instantly dispersed in the reactive medium and consumed by borate ions according to the neutralization reaction (Eq. 12) which is infinitely faster than the second reaction (Eq. 13). When the mixing process is slow, a local excess of H^+ ions can occur, allowing the production of iodine.[58]

These experiments were carried out using a small variation on the method by Guichardon[58] as described in Siddiqui.[62] Sulfuric acid (0.5M) was injected by a positive displacement pump (Ismatec) from a 250 mL glass beaker through a 3 mm diameter stainless steel nozzle into the tank. The flow rate was 60 mL/min, and the weight of the injected sulfuric acid was measured by the difference. Each measurement was carried out twice with 20 mL of the sulfuric acid solution injected each time. Temperature and pH were monitored via probes immersed in the tank. The initial pH for each experiment was 9.03 and the initial temperature was between 294.7 and 296.2 K. After the addition of the sulfuric acid, the pH dropped to between 8.95 and 8.99 with a final temperature between 294.8 and 296.3 K. A spectrophotometer (Ocean Optics, model SQ 2000) was used to measure the concentration of triiodide ion in the tank. The *in situ* probe (5 mm optical path length) monitored the 352 nm wavelength for iodine. The results are given in terms of the percent of the maximum yield of desired product (Y_S, Y_B, and Y_I).

Results

The results are divided into five parts. In the first and second parts, the hydrodynamic characteristics of the impellers are presented: power number, flow number, momentum number, and local dissipation. In the other three parts, the focus is on the mixing performance of the impellers. The discussion of the results addresses two areas of interest: the performance of the KPC compared to the PBT, and the usefulness of the different measurements for impeller comparison.

Power number

The power number is currently the primary point of comparison between impellers. The experimental method is well established and repeatable across several laboratories and the value (N_p) is used in a wide range of design correlations. It is clearly an important impeller characteristic.

Figure 3 presents the power number curves for an off-bottom clearance of $C = T/3$. In fully turbulent flow ($Re = 2.0 \times 10^4$ for PBT and $Re > 4.0 \times 10^4$ for KPC) the power number is independent of *Re*. The fully turbulent N_p results for the PBT, given in Table 3, are within 4% of power numbers reported by Hemrajani[9] and are close to the power

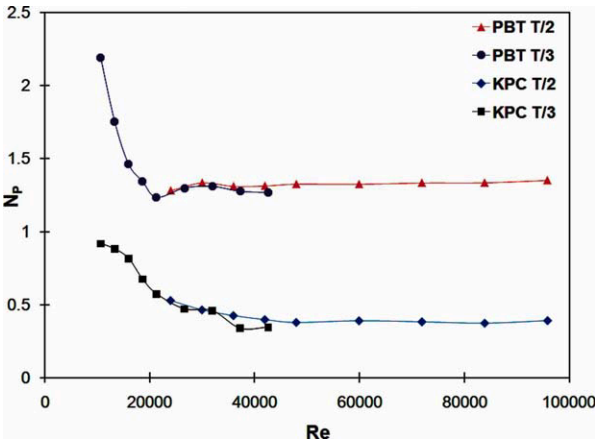

Figure 3. The transition of N_P to fully turbulent flow: for the PBT, N_P is constant for $Re > 20\ 000$; but for the KPC, N_P continues to drop until $Re > 40\ 000$.

[Color figure can be viewed in the online issue, which is available at wileyonlinelibrary.com.]

Table 3. Impeller Dimensions and Power, Pumping and Momentum Number Results

Impeller, D	Diameter (mm)	Blade width (mm)	C/T	Re	N_P	N_Q	Mo
PBT T/2	121.6	25.2	0.25	$4.8x10^4$	1.37	0.80	0.90
				$3.2x10^4$	1.37	0.80	0.91
			0.33	$4.8x10^4$	1.32	0.80	0.87
				$3.2x10^4$	1.32	0.78	0.87
PBT T/3	78.5	15.9	0.25	$4.8x10^4$	1.34	0.73	0.80
				$3.2x10^4$	1.34	0.71	0.78
			0.33	$4.8x10^4$	1.29	0.72	0.77
				$3.2x10^4$	1.29	0.70	0.74
KPC T/2	119.4	Not specified	0.25	$4.8x10^4$	0.41	0.50	0.36
				$3.2x10^4$	0.41	0.49	0.35
			0.33	$4.8x10^4$	0.39	0.48	0.35
				$3.2x10^4$	0.41	0.47	0.33
KPC T/3	78.2	Not specified	0.25	$4.8x10^4$	0.40	0.47	0.33
				$3.2x10^4$	0.46	0.46	0.33
			0.33	$4.8x10^4$	0.36	0.45	0.32
				$3.2x10^4$	0.46	0.45	0.31

numbers predicted by Chapple[2] (13% for D = T/2 and 2% for D = T/3).

The power number is a strong function of impeller geometry. While there are cases where the power number is independent of the tank configuration, the power number can also be sensitive to the impeller diameter, off-bottom clearance, baffle configuration, and Reynolds number. Chapple[2] found that the power number of the PBT depends on the impeller to tank diameter ratio, but these new results show only a small effect of diameter for both impellers. Table 3 also presents power numbers measured at a clearance of C = T/4. The power numbers were only slightly higher when the impellers were located closer to the bottom of the tank. Armenante[5,68] found a similar behavior. The fully turbulent power number should always be reported with the key geometric variables and can only safely be applied when geometric similarity is strictly obeyed. Accurate measurement of the impeller diameter is particularly important.

Pumping and momentum number

The flow number and the momentum number were calculated from profiles of the mean axial velocity in the impeller discharge stream. Figure 4 compares the turbulent power number, flow number and momentum number for all four impellers at C = T/3 and fully turbulent flow. The power number is an average of all of the fully turbulent values from Figure 3. The pumping and the momentum numbers are an average of all configurations for each impeller. The error bars on the pumping and momentum numbers show that when *Re* and C/T were varied the changes in N_Q and *Mo* were small. When the PBT diameter drops from D = T/2 to D= T/3; however, the flow number drops by 11.25%, and the momentum number drops by 15%. The effect of the diameter was smaller for the KPC (flow number drops by 6.25%, and momentum number drops by 8.6% from T/2 to T/3).

Table 3 shows the results for all of the configurations and Reynolds numbers tested. Both the pumping and momentum number depend on the shape of the impeller and on the impeller diameter. The clearance and the Reynolds number have a small effect on the results. According to Hemrajani,[9] the PBT has a constant flow number for *Re* higher than 10 000. Wu[18] reported that the PBT (C/T = 0.33 and D/T = 0.41) has a flow number of 0.76, which agrees with the results presented in this work. There are no published data for the KPC impeller, but other hydrofoil impellers have flow numbers varying from 0.55 to 0.73,[9,16,18] which is higher than the results obtained here.

The constant of proportionality obtained in Eq. 8 is compared with the new experimental data in Figure 5. The experimental best fit constant is 1.45 with a correlation coefficient of 0.989, which is close to the estimate of 1.43 from Eq. 8. Brown[26] obtained a correlation of 0.99 with a constant of 1.46 for six different shapes of impellers (HE3, A310, LE20, 3SHP1, A320 and PBT 45°), with D = T/2 and D =

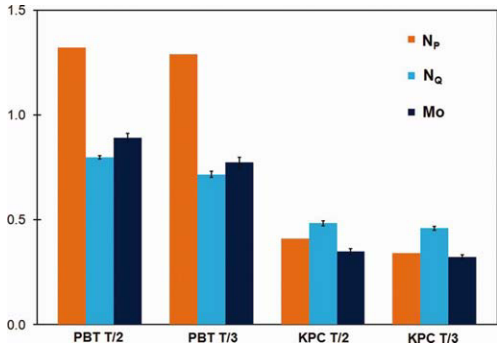

Figure 4. Comparison of power number, flow number, and momentum number in the fully turbulent regime.

The error bars on N_Q and *Mo* show the small variance between cases. [Color figure can be viewed in the online issue, which is available at wileyonlinelibrary.com.]

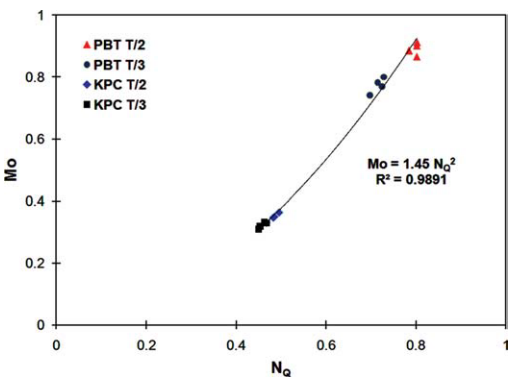

Figure 5. Comparison of experimental data for *Mo* with Eq. 8 based on N_Q.

[Color figure can be viewed in the online issue, which is available at wileyonlinelibrary.com.]

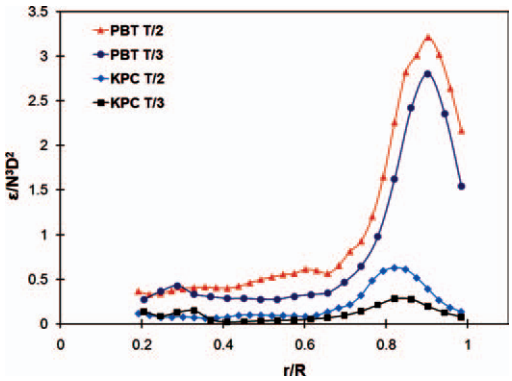

Figure 6. Dimensionless profiles of the rate of dissipation of turbulent kinetic energy 3 mm below the impeller.

[Color figure can be viewed in the online issue, which is available at wileyonlinelibrary.com.]

T/3. Based on the results obtained in this work and on the results reported by Brown,[26] it is concluded that the momentum number can be calculated from the flow number, and vice versa, using either the 1.46 constant from Brown's data, or the constant found in this work:

$$\mathrm{Mo} = 1.45\mathrm{N}_\mathrm{Q}^2 \tag{15}$$

These results also show that the momentum number and the flow number are interchangeable, so a single integration can be used to find both and historical data for N_Q can be used to find *Mo*. The authors recommend the use of *Mo*, since the momentum in a jet is conserved as the impeller discharge jet expands into the bulk of the tank, while the volumetric flow rate increases as fluid is entrained. The fact that *Mo* has been successfully used in a number of correlations suggests that it has the potential for wider use as an impeller characteristic.

Estimates of the local dissipation rate of turbulent kinetic energy

Figure 6 shows profiles of the dimensionless turbulent kinetic energy dissipation rate (ε/N^3D^2) for all four impellers. The scaling of the dissipation with N^3D^2 arises from making Eq. 9 dimensionless with the characteristic length (D) and velocity (ND) scales for a stirred tank. The results for the PBT match the peak values reported by Zhou[31] with $\varepsilon_{max}/N^3D^2 = 3.3$ for PBT T/2, 2.7 for PBT T/3, 0.8 for KPC T/2 and 0.3 for KPC T/3.

The dimensionless dissipation results suggest that large impellers generate more turbulence, but when the dimensionless scaling is removed and *Re* is held constant, as shown in Table 1, the conclusion changes and the smaller impellers appear to generate more turbulence. Clearly, the correct design approach is to determine the required dissipation based on process objectives, and then set the operating conditions to achieve it.

Since the local maximum dissipation ε_{max}, determines the outcome of several process objectives, such as micromixing and drop size, it should be included as a standard impeller characteristic. As with all other impeller characteristics, the dissipation profiles should be reported with the details of the tank configuration used to collect the data. Either a standard tank geometry such as the one reported here, or a geometry specified to optimize the performance of the impeller should be selected for the measurements.

Just suspended speed and power at just suspended speed

The just suspended speeds for two different solids are shown in Figure 7. In Figure 7a, the N_{js} results for 3 wt % glass beads are shown. The PBT has a smaller N_{js} than the KPC for the same conditions. N_{js} increases when the clearance increases, and decreases when the diameter increases. In Figure 7b, the *Njs* results for 3 wt % bronze powder are shown. The speeds are significantly higher because the density is higher, but the effects of varying clearance, diameter, and impeller type are similar. The KPC T/3 impeller could not achieve solids suspension for bronze at high clearances because the maximum speed of the motor (1739 rpm) was exceeded.

In Figure 8, P_{js} is compared for the four impellers and the two solids tested. In these figures, some new information emerges. The power consumption is roughly 30 times higher for the bronze particles than for the glass, compared to N_{js}, which is three times higher. Power scales as N^3, so this is exactly as expected. The point is an important one for industrial application: suspension of dense solids is a power intensive operation, so for solids suspension, direct comparison of power is more fruitful than comparison of N_{js}. Turning to the results, N_{js} was higher for the KPC, but P_{js} is the lowest for the D = T/3 KPC. The D = T/2 KPC does well with the glass beads, but not as well for the bronze. It appears that

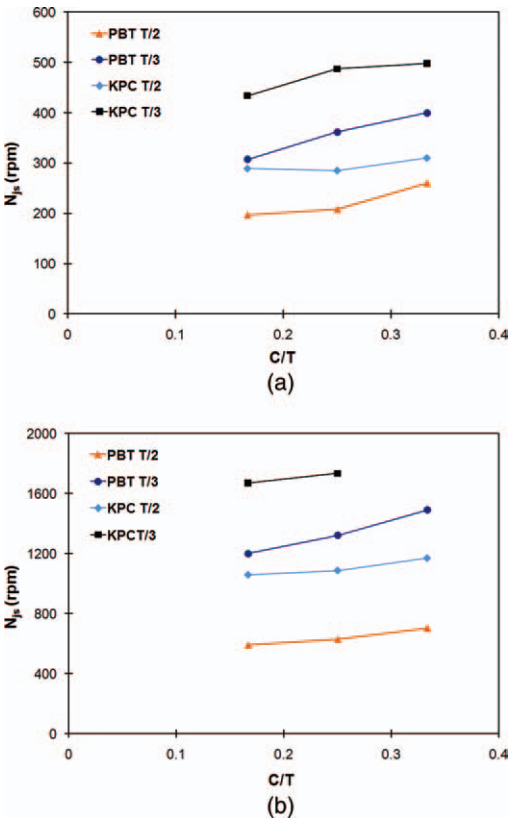

Figure 7. (a) Just suspended speed (N_{js}) using 3 wt % glass beads; (b) just suspended speed (N_{js}) using 3 wt % bronze powder.

[Color figure can be viewed in the online issue, which is available at wileyonlinelibrary.com.]

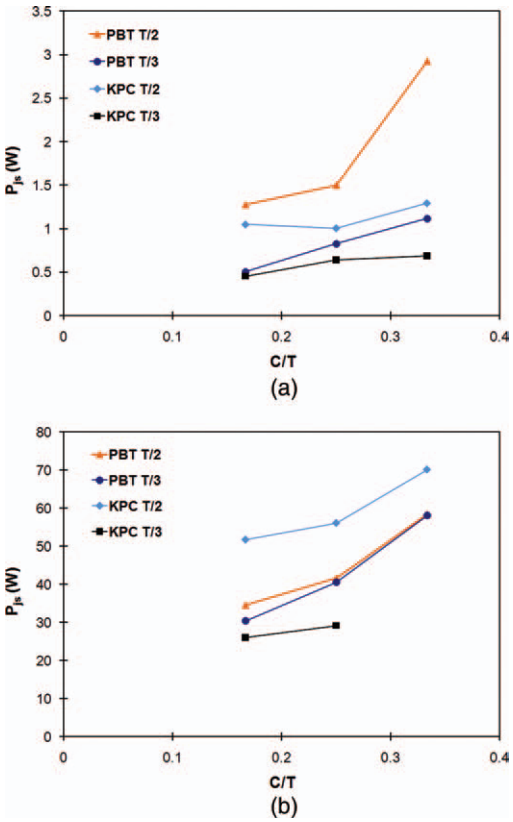

Figure 8. (a) Power consumption at just suspended speed using 3 wt % glass beads.

The mass of the slurry in the tank was 11.06 kg. (b) Power consumption at just suspended speed using 3 wt % bronze powder. The mass of the slurry in the tank was 11.20 kg. [Color figure can be viewed in the online issue, which is available at wileyonlinelibrary.com.]

the bronze particles need more turbulence to be suspended and this can be provided more easily by the PBT than the KPC. The glass beads are less dense; therefore, the turbulence is not as necessary and the high-flow KPC gives a better performance.[69] Overall the D = T/2 impellers consume more power at N_{js} than the D = T/3 impellers. From experimental observations and a survey of published data by Ayranci,[53] large impeller diameter ratios are inefficient for solid suspension because suspending the particles below the shaft becomes more difficult as the D/T ratio increases.

The effect of particle type on impeller performance also appears in the Zwietering constant S_Z. Figure 9 compares values of S_Z calculated for glass and for bronze in a parity plot. For the D = T/2 impellers, the S_Z values are quite similar for glass and bronze, but for the D = T/3 impellers there are significant differences between the two sets of results. This is an unexpected outcome which suggests that important factors related to the particle properties may be missing from the Zweitering equation. Ibrahim[70] also compared the suspension of glass beads and bronze particles and the bronze particles tended to have bigger S_Z values than glass beads when all other conditions were held constant.

Solids suspension performance was used to compare impellers based on their ability to generate flow and turbulence at the bottom of the tank. The N_{js}, P_{js}, and S_Z comparisons gave different conclusions. The most important operational point is P_{js}, because solids suspension is power intensive. The main conclusion from the power comparison is that smaller impellers are more efficient. The parity plot of S_Z values revealed that for smaller impellers, the S_Z value depends on the particles used. Since the S_Z value is known to contain a number of geometric interactions which are convoluted into one variable, while P_{js} is an unambiguous measure of performance, P_{js} is recommended as the primary measure of performance for solids suspension.

Air entrainment speed

The influence of impeller submergence on N_E is shown in Figure 10 for all four impellers. The point of air entrainment N_E is affected by both the type of impeller and the impeller diameter. An increase in submergence causes an increase in N_E. Bhattacharya[55] made the same conclusion for four different fluids and two impeller sizes. As the submergence is increased the turbulent energy reaching the surface drops, and a higher impeller speed is needed to form bubbles at the liquid surface. The T/3 KPC impeller shows a large jump in N_E from S/T = 0.25 to S/T = 0.29; after this, N_E is constant. The sudden jump occurs due to a change in flow pattern at $S/T = 0.25$. The large impellers have a smaller N_E and are less sensitive to submergence. Comparing impellers with same diameter, the PBT has a smaller N_E than the KPC. This suggests a direct comparison of the power consumption at the point of air entrainment.

Figure 11 shows the power consumption for all four impellers which was calculated using the power numbers reported in Table 3. As expected, the power consumption increases when the submergence increases. The small PBT consumes the most energy, but the difference between the impellers is relatively small when S/T $<$ 0.25. When a submergence larger than S/T = 0.3 is used, the conditions at the surface vary significantly between impellers.

Comparing the results shown in Figure 11 for mixing close to the surface of the tank (P_E) with the results shown in Figure 8 for mixing close to the bottom of the tank (P_{js}), a somewhat obvious conclusion emerges: performance is better when the impeller is close to where mixing is needed. Large impellers are better at air entrainment, while

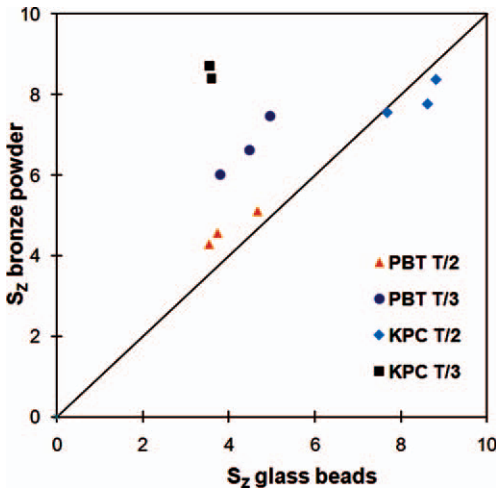

Figure 9. Comparison of the *S* values from Eq. 10 for glass beads and bronze powder with all other experimental conditions matched.

[Color figure can be viewed in the online issue, which is available at wileyonlinelibrary.com.]

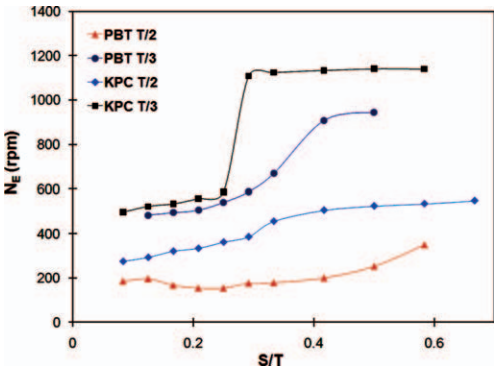

Figure 10. N_E as a function of the impeller submergence.

[Color figure can be viewed in the online issue, which is available at wileyonlinelibrary.com.]

small impellers are more efficient for solids suspension. If both air entrainment and solids suspension are required for the same application, two impellers might reasonably be specified: a large one close to the surface for gas entrainment and a small one close to the bottom for solids suspension. Final selection would require a reasonable match between N_E and N_{js}. The power consumption at N_E for all four impellers is similar for $S < 0.25$T while N_E varies, so for the case where air entrainment is desired, N_E is the better choice for impeller comparison and the large PBT gives the best performance (lowest N_E and smallest power consumption). Where air entrainment is not desired, a submergence $S > 0.25$T should be selected and the small KPC gives the best performance, quickly achieving the maximum N_E, which is the maximum resistance to air entrainment. For both air entrainment cases, N_E is the best choice for impeller comparison.

Micromixing efficiency

The final set of tests in the protocol is the yield of a micromixing limited reaction using three different feed points (Y_S, Y_B, and Y_I) and three scaling methods.

- In the first scaling, the Reynolds number is held constant ($Re = 20\,000$) to compare impeller performance in the same flow regime.
- In the second scaling, micromixing tests are carried out at the point of air entrainment (N_E) to compare micromixing performance with surface feed.
- The third scaling is based on constant power per mass of fluid ($P/\rho V_{\text{tank}}$) with analysis of the results using two other measures of turbulence: power per mass of fluid in the impeller swept volume ($P/\rho V_{\text{swept}}$), and maximum local dissipation ($\varepsilon_{\max}$) from Figure 6, all in (W/kg).

The results are shown in Figures 12 and 13, with the first two scaling approaches (Re and N_E) in Figure 12a and b, and the constant power per mass results in Figure 13a and b. First the yields are compared for each configuration and then parity plots provide a paired comparison of the KPC and the PBT at the same conditions (C, D, feed point and either $Re = 20\,000$, N_E or same power per mass).

Figure 12a presents the $Re = 20\,000$ results on the left half of the graph, with the N_E results on the right. The yield of the desired products varies from 90.7% to 97.6% of the maximum. This range of yields is similar to that found by Siddiqui[62] for the same iodide-iodate reaction. At constant Re, the PBT gave larger yields than the KPC because it has a higher N_p and a larger maximum dissipation. Increases in both N_p and ε give more intense micromixing, particularly close to the impeller. The lowest yields were obtained for surface feed and feed close to the baffle with the low turbulence, high-efficiency KPC. At the point of air entrainment, the results scale well for the surface feed location but vary significantly for the impeller feed and the baffle feed locations. This suggests that if a surface feed cannot be avoided, scale-up based on N_E with impeller selection based on P_E can be effective. As expected, the yield for surface feed is lower than the yield for feed at the impeller.

Figure 12b shows parity plots for constant Re and for N_E. When a data point is above the diagonal, the PBT performs better; when a point is below the diagonal, the KPC performs better. At constant Re, the PBT performs better than the KPC, but since this scaling is biased toward the higher power number impeller, this is a flaw in the scaling, not a reflection on the impeller. The N_E condition gives similar performance for both impellers only when the surface feed is used. The point of air entrainment provides approximately the same turbulence level at the surface. When the reactants are fed at the impeller with $N = N_E$, the PBT gives a higher yield. This emphasizes that while the turbulence at the surface is the same at N_E, the turbulence close to the impeller is likely to be quite different. The point of air entrainment should not be used as a scaling approach for feed at the impeller.

The results of the third scaling approach, constant $P/\rho V_{\text{tank}}$, are shown in Figure 13a. The yields vary from 91.3% to 96.0% across the three feed locations and four impellers. On the left, the yields obtained at high power are shown; while on the right, the results for low power are shown. Power consumption is clearly the most important effect in micromixing experiments. When more power per mass is consumed, there is more energy dissipation and the yield increases. At lower power consumption, the variation of the results is wider and the yield is consistently lower. The feed location with the lowest yield is consistently the surface feed, with the highest yields obtained for feed at the impeller. Figure 13b shows that the apparent difference between impellers disappears when the scaling is based on equal power per mass. This is clearly the most reliable of the three scaling methods.

The next question related to this set of experiments is whether the micromixing experiments provide additional and reliable information for impeller comparison. In Figure 14,

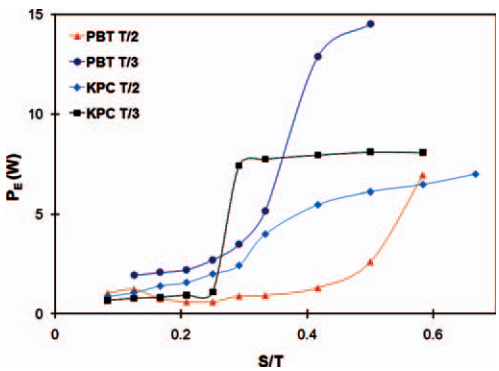

Figure 11. Power consumption calculated at the point of air entrainment as a function of submergence.

[Color figure can be viewed in the online issue, which is available at wileyonlinelibrary.com.]

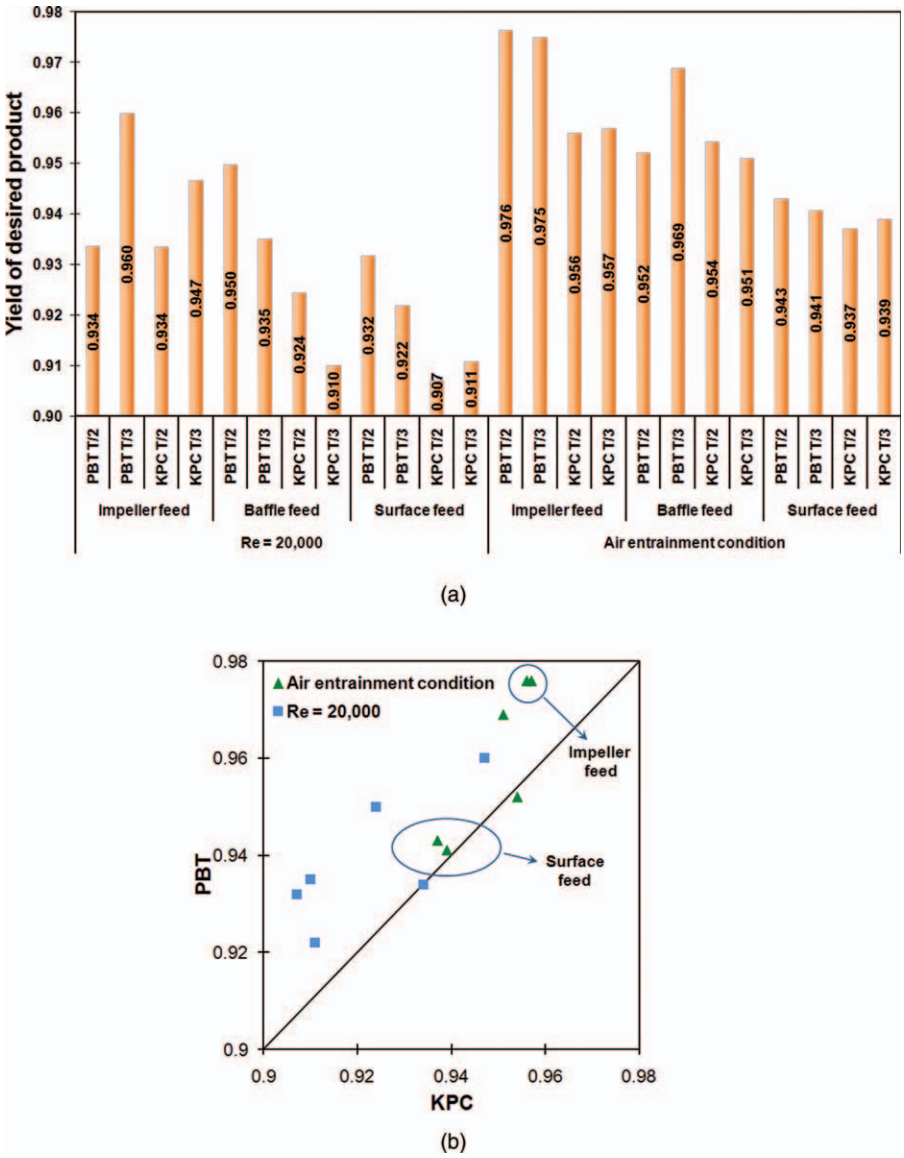

Figure 12. (a) Yield of desired product at *Re* = 20 000 and at the point of air entrainment.

Three feed locations and four impellers are compared. (b) Comparison of the yield for the PBT and the KPC impellers for Re 20 000 and at the point of air entrainment. The point of air entrainment gives good scaling for a surface feed. [Color figure can be viewed in the online issue, which is available at wileyonlinelibrary.com.]

the yield is plotted against the peak local dissipation (ε_{max} from Figure 6) for all 16 impeller feed experiments. This is a more precise scaling of reaction feed conditions than the average power dissipation across the tank volume ($P/\rho V_{tank}$). The yield is correlated to the local maximum dissipation at lower levels of dissipation but once the micromixing limit is achieved the yield remains constant even while the local dissipation at the feed point continues to increase. It is concluded that while micromixing experiments provide crucial mixing information for process development and scale-up, they are not reliable for direct comparison of impellers.

The final observations from the micromixing experiments consider all 16 impeller feed experiments which are plotted together in Figure 14 with Y_I as a function of ε_{max}. When a peak energy dissipation greater than 1 W/kg is used, the yield is constant as was also seen for the high power case in Figure 13a. One very high yield (>0.97) occurs for impeller feed under the N_E condition when the dissipation is very high (14 W/kg). The other was replicated several times but is not easily explained. For dissipation <1 W/kg, the yield is correlated to the local dissipation, not to ($P/\rho V_{tank}$). This is also seen for the low power impeller feed case in Figure 13, where ($P/\rho V_{tank} = 0.011$ W/kg) for all experiments, but the yield varies. Returning to Table 2 for the low-power data, ($P/\rho V_{swept}$) reveals two pairs of data, one close to 2 W/kg for the D = T/3 impellers and the other close to 0.7 W/kg for the D = T/2 impellers. The low ($P/\rho V_{swept}$) data also gave a lower yield. We conclude that ($P/\rho V_{swept}$) correctly accounts for the effect of impeller diameter. Taking the comparison to the next level of detail requires ε_{max} information, as shown in Figure 14. Given ε_{max}, the feed conditions for geometries which are significantly different can be directly compared. In summary, either ($P/\rho V_{swept}$) or ε_{max} is recommended for scaling of a final design, but the micromixing experimental results (Y_I, Y_S, Y_B) did not add any new information to a comparison of the impellers.

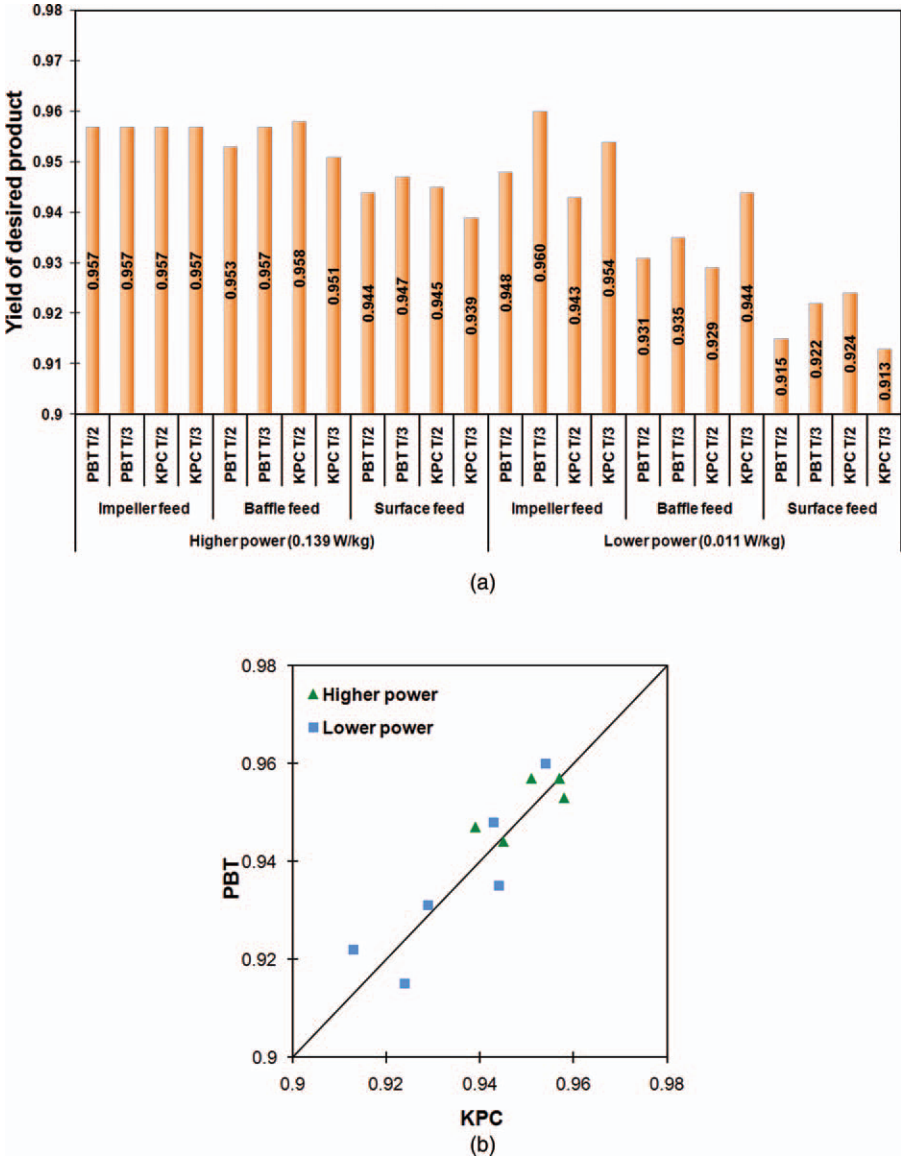

Figure 13. (a) Yield of desired product for two levels of power per mass.

Three feed locations and four impellers are compared. (b) Comparison of the yield of desired product for the PBT and the KPC at high- and low-power input. The performance is equivalent using this scaling, with the highest yield for high power and feed at the impeller. [Color figure can be viewed in the online issue, which is available at wileyonlinelibrary.com.]

Conclusions

The objective of this work was to select a set of measurements which define a protocol for comparison of impellers in turbulent mixing. Comparing impellers based on a single criterion or test geometry is not sufficient, since a mixing tank is a complex vessel where several competing process objectives often coexist. To characterize a mixing configuration, it is necessary to collect information from several different parts of the tank: the impeller region, the bottom of the tank and the liquid surface.

Starting with the impeller region, the power number was confirmed as the most important characteristic of an impeller. It was shown that the momentum number Mo, can be calculated from N_Q, but Mo is recommended over N_Q, because momentum is conserved in the impeller discharge stream and flow is not. The third characteristic of impeller performance close to the impeller is an estimate of ε_{max}/N^3D^2, as this gives the most accurate prediction of micromixing performance close to the impeller. If ε_{max}/N^3D^2 and Mo cannot be measured, $P/\rho V_{swept}$ is preferable to $P/\rho V_{tank}$ as a scaling variable for turbulence intensity at the impeller.

In the bulk of the tank, the bottom and the surface gave the most meaningful results. For solids suspension from the bottom of the tank, P_{js} gave the most direct comparison of performance. The just suspended speed is neither the process objective nor the point of optimal performance and the Zweitering constant S_Z, depended on the particle type, particularly for the smaller impellers. The later result is surprising and suggests that the correlation is missing some important aspect of the physics. To minimize P_{js}, a small impeller with a small off-bottom clearance should be selected, but to minimize P_E, a large impeller with small submergence is needed. The point of air entrainment, N_E, gave more informative comparisons

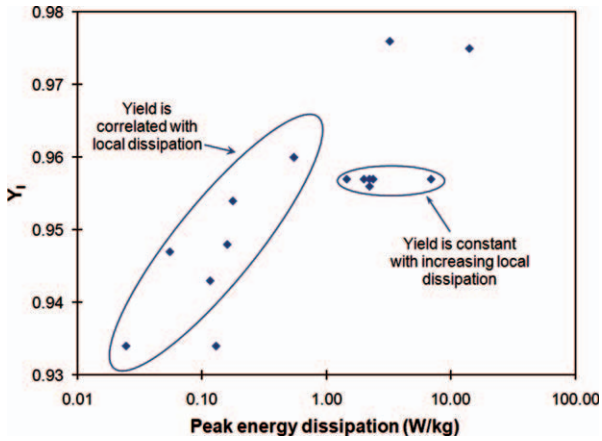

Figure 14. Using micromixing performance as a measure of local dissipation is meaningful only below the micromixed limit.

[Color figure can be viewed in the online issue, which is available at wileyonlinelibrary.com.]

for conditions at the surface than P_E because P_E is similar for all impellers for $S = 0.25$. The micromixing experiments did not provide any additional insights with respect to impeller characterization, but they did provide some information about the best approaches to use for scale-up and design of reactors.

A set of five variables is recommended to characterize a new impeller: the power number N_p, the momentum number Mo, the maximum dimensionless local dissipation, ε_{max}/N^3D^2, the power consumption at just suspended speed P_{js}, and the rotational speed at the point of air entrainment N_E. Using these criteria, the full range of impeller performance and its impact on different regions in the mixing tank can be defined, allowing the most suitable geometry to be selected for the application of interest. In all cases, the impeller performance is sensitive to D/T, C/T and S/T, so the tank configuration is an important part of the design specification.

Considering the two impellers which were the subject of this study, the results confirmed that the blade geometry is important. The PBT impeller consumes more power than the KPC and provides more turbulence to the flow. On the other hand, the KPC provides more momentum than PBT for the same power consumption. Power consumption at just suspended speed favors the KPC, and the KPC was able to operate at higher rotational speeds without air entrainment. Conversely, the PBT consumes less power at the point of air entrainment. In short, both impellers have advantages and disadvantages, so the choice of impeller depends on the requirements of the mixing process.

Acknowledgments

The authors thank the CNPq (Conselho Nacional de Desenvolvimento Científico e Tecnológico - Brazil), the Alberta Ingenuity Fund, the Natural Sciences and Research Council (NSERC) of Canada, and the Canadian Foundation for Innovation for financial support, Kroma Equipamentos Industriais LTDA for the impellers and Adam Madej for technical support and data processing for stereo PIV.

Notation

Roman characters

A = constant in Eq. 9
A = area in Eq. 3
b = slope of the velocity profile segment
C = off-bottom clearance, m
D = impeller diameter, m
d_P = particle diameter, m
F_z = axial thrust on the impeller due to acceleration of fluid, N
g = acceleration due to gravity, m s^{-2}
H = total liquid level, m
L = turbulent integral length scale, m
L_{res} = 3-D resultant macrolength scale
n = normal direction to the surface area, m
N = impeller rotational speed, s^{-1}
N_E = air entrainement speed, s^{-1}
N_{js} = just suspended speed, s^{-1}
Mo = momentum number
N_P = power number
N_Q = flow number, also called the Pumping number in some references
P = power, W
P_E = power consumption at the point of air entrainment, W
P_{js} = power at just suspended speed, W
Q_{imp} = volumetric flow rate at the impeller discharge cross section, m^3 s^{-1}
Q_{jet} = volumetric flow rate of the jet reaching the baffles, m^3 s^{-1}
q = turbulent kinetic energy, m^2 s^{-2}
r = radius, m
Re = reynolds number
S = submergence, m
S_Z = Zwietering constant in N_{js} correlation
T = tank diameter, m
u' = rms of the fluctuating velocity component in the main flow direction, m s^{-1}
V_z = axial velocity, m s^{-1}
V_{tank} = tank volume, m^3
V_{swept} = impeller swept volume, m^3
w = blade width, m
w_b = baffle width, m
X = solids loading, mass of solid/mass of liquid × 100
Y_S, Y_B, Y_I = yield for surface feed, baffle feed, and impeller feed

Greek letters

ε = rate of dissipation of turbulent kinetic energy, m^2 s^{-3}
ε_{max} = peak value of dissipation rate of turbulent kinetic energy, m^2 s^{-3}
ν = kinematic viscosity of water, m^2 s
ρ = density, g m^{-3}
ρ_L = liquid density, g m^{-3}
ρ_S = solid density, g m^{-3}
ρ_{slurry} = slurry density, g m^{-3}

Abbreviations

B = bronze
G = glass beads
KPC = Kroma KPC impeller
LDA = laser doppler anemometry
PBT = pitched blade turbine
PIV = particle image velocimetry

Literature Cited

1. Dickey DS, Fenic JC. Dimensional analysis for fluid agitation systems. *Chem Eng*. 1976(1);83:139–145.
2. Chapple D, Kresta SM, Wall A, Afacan A. The effect of impeller and tank geometry on power number for a pitched blade turbine. *Chem Eng Res Des*. 2002;80(4):364–372.
3. Rushton JH, Costich EW, Everett HJ. Power characteristics of mixing impellers. *Chem Eng Progr*. 1950;46:395–404, 1950;46:467–479.
4. Bates RL, Fondy PL, Corpstein RR. An examination of some geometric parameters of impeller power. *IEC Process Des Develop*. 1963;2(4):310–314.
5. Armenante PM, Mazzarotta B, Chang GM. Power consumption in stirred tanks provided with multiple pitched-blade turbines. *Ind Eng Chem*. 1999;38:2809–2816.
6. Dickey DS, Patterson GK. Find mixing success through failures: Part 1. *Chem Eng Progr*. 2008;104(10):40–47.
7. Fujasová M, Linek V, Moucha T. Mass transfer correlations for multiple-impeller gas-liquid contactors. Analysis of the effect of

axial dispersion in gas and liquid phases on "local" kLa values measured by the dynamic pressure method in individual stages of the vessel. *Chem Eng Sci*. 2007;62(6):1650–1669.
8. Nocentini M, Magelli F, Pasquali G, Fajner D. A fluid-dynamic study of a gas liquid, non-standard vessel stirred by multiple impellers. *Chem Eng J*. 1988;37:53–59.
9. Hemrajani RR, Tatterson GB. *Mechanically stirred vessels*. In: Paul EL, Atiemo-Obeng VA, Kresta. SM, eds. *Handbook of Industrial Mixing: Science and Practice*: John Wiley & Sons, Inc.; 2004.
10. Fořt I. *Flow and turbulence in vessels with axial impellers*. In: Uhl VW, Gray JB, eds. *Mixing: Theory and Practice*. 1986;3:133–197.
11. Weetman RJ, Oldshue JY. Power, flow and shear characteristics of mixing impellers. *Sixth European Conference on Mixing*. Pavia, Italy: BHRA, the Fluid Engineering Centre, Cranfield, United Kingdom 1988.
12. Ranade VV, Joshi JB. Flow generated by pitched blade turbines I: Measurements using laser doppler anemometer. *Chem Eng Commun*. 1989;81(1):197–224.
13. Kresta SM, Wood PE. The mean flow field produced by a 45° pitched blade turbine: Changes in the circulation pattern due to off bottom clearance. *Can J Chem Eng*. 1993;71:42–53.
14. Rutherford K, Lee KC, Mahmoudi SMS, Yianneskis M. Hydrodynamic characteristics of dual Rushton impeller stirred vessels. *AIChE J*. 1996;42(2):332–346.
15. Sahu AK, Kumar P, Patwardhan AW, Joshi JB. CFD modelling and mixing in stirred tanks. *Chem Eng Sci*. 1999;54:2285–2293.
16. Wu J, Pullum L. Performance analysis of axial-flow mixing impellers. *AIChE J*. 2000;46(3):489–498.
17. Aubin J, Mavros P, Fletcher D, Bertrand J, Xuereb C. Effect of axial agitator configuration (up-pumping, down-pumping, reverse rotation) on flow patterns generated in stirred vessels. *Chem Eng Res Des*. 2001;79(8):845–856.
18. Wu J, Zhu Y, Pullum L. Impeller geometry effect on velocity and solids suspension. *Chem Eng Res Des*. 2001;79(8):989–997.
19. Spogis N, Nunhez JR. Design of a high-efficiency hydrofoil through the use of computational fluid dynamics and multiobjective optimization. *AIChE J*. 2009;55(7):1723–1735.
20. Fořt I. On hydraulic efficiency of pitched blade impellers. *Chem Eng Res Des*. 2011;89(6):611–615.
21. Kresta S, Anthieren G, Parsiegla K. Mixing effects in silver halide precipitation linking theory with practice using a multi-mechanism model. *Chem Eng Res Des*. 2004;82(9):1117–1136.
22. Grenville RK, Musgrove ME, Fawcett NSJ. The relationship between turbulent blend time and momentum generated by impellers and jet mixers. Paper presented at: 17th North American Mixing Forum 1999; Banff, Alberta, Canada.
23. Bhole M, Ford C, Bennington CPJ. Characterization of Axial Flow Impellers in Pulp Fibre Suspensions. Paper presented at: 13th European Conference on Mixing; 14–17 April, 2009; London, UK.
24. Jones PN, Özcan-Taşkin NG, Yianneskis M. The use of momentum ratio to evaluate the performance of CSTRs. *Chem Eng Res Des*. 2009;87(4):485–491.
25. Kresta S, Wood P. Prediction of the three-dimensional turbulent flow in stirred tanks. *AIChE J*. 1991;37(3):448–460.
26. Brown DAR. Mixer performance characteristics: Impeller and process efficiency. Paper presented at: 22nd North American Mixing Forum 2010; Victoria, BC, Canada.
27. Escudié R, Liné A. Experimental analysis of hydrodynamics in a radially agitated tank. *AIChE J*. 2003;49(3):585–603.
28. Wu H, Patterson GK. Laser-doppler measurements of turbulent-flow parameters in a stirred mixer. *Chem Eng Sci*. 1989;44(10):2207–2221.
29. Delafosse A, Collignon M-L, Crine M, Toye D. Estimation of the turbulent kinetic energy dissipation rate from 2D-PIV measurements in a vessel stirred by an axial mixel TTP impeller. *Chem Eng Sci*. 2011;66:1728–1737.
30. Delafosse A, Line A, Morchain J, Guiraud P. LES and URANS simulations of hydrodynamics in mixing tank: Comparison to PIV experiments. *Chem Eng Res Des*. 2008;86(12):1322–1330.
31. Zhou G, Kresta SM. Impact of tank geometry on the maximum turbulence energy dissipation rate for impellers. *AIChE J*. 1996;42(9):2476–2490.
32. Kresta SM, Wood PE. The flow field produce by a pitched blade turbine: characterization of the turbulence and estimation of the dissipation rate. *Chem Eng Sci*. 1993;48(10):1761–1774.
33. Cutter LA. Flow and turbulence in a stirred tank. *AIChE J*. 1966;12(1):35–45.
34. Okamoto Y, Nishikawa M, Hashimoto K. Energy dissipation rate distribution in mixing vessels and its effects on liquid-liquid dispersion and solid-liquid mass transfer. *Int Chem Eng*. 1981;21(88):88–94.
35. Zhou G, Kresta SM. Distribution of energy between convective and turbulent flow for three frequently used impellers. *Chem Eng Res Des*. 1996;74(3):379–389.
36. Ducci A, Yianneskis M. Direct determination of energy dissipation in stirred vessels with two-point LDA. *AIChE J*. 2005;51(8):2133–2149.
37. Baldi S, Ducci A, Yianneskis M. Determination of dissipation rate in stirred vessels through direct measurement of fluctuating velocity gradients. *Chem Eng Technol*. 2004;27(3):275–281.
38. Roussinova V, Grgic B, Kresta S. Study of macro-instabilities in stirred tanks using a velocity decomposition technique. *Chem Eng Res Des*. 2000;78(7):1040–1052.
39. Khan F, Rielly C, Brown D. Angle-resolved stereo-PIV measurements close to a down-pumping pitched-blade turbine. *Chem Eng Sci*. 2006;61(9):2799–2806.
40. Kresta SM, Brodkey RS. *Turbulence in Mixing Applications*. In: Paul EL, Atiemo-Obeng VA, Kresta SM, eds. *Handbook of Industrial Mixing: Science and Practice*: John Wiley & Sons, Inc.; 2004.
41. Baldyga J, Bourne JR, Hearn SJ. Interaction between chemical reactions and mixing on various scales. *Chem Eng Sci*. 1997;52(4):457–466.
42. Barrett M, OGrady D, Casey E, Glennon B. The role of meso-mixing in anti-solvent crystallization processes. *Chem Eng Sci*. 2011;66:2523–2534.
43. Baldyga J, Bourne JR, Yang Y. Influence of feed pipe diameter on mesomixing in stirred tank reactors. *Chem Eng Sci*. 1993;48(19):3383–3390.
44. Torbacke M, Rasmuson ÅC. Influence of diferent scales of mixing in reaction crystallization. *Chem Eng Sci*. 2001;56:2459–2473.
45. Torbacke M, Rasmuson ÅC. Mesomixing in semi-batch reaction crystallization and influence of reactor size. *AIChE J*. 2004;50(12):3107–3119.
46. Li S, Xu J, Wang Y, Luo G. Mesomixing scale controlling and its effect on micromixing performance. *Chem Eng Sci*. 2007;62:3620–3626.
47. Grenville RK, Nienow AW. *Blending of miscible liquids*. In: Paul EL, Atiemo-Obeng VA, Kresta SM, eds. *Handbook of Industrial Mixing: Science and Practice*: John Wiley & Sons, Inc.; 2004.
48. Atiemo-Obeng VA, Penney WR, Armenante P. *Solid-liquid mixing*. In: Paul EL, Atiemo-Obeng VA, Kresta SM, eds. *Handbook of Industrial Mixing: Science and Practice*: John Wiley & Sons, Inc.; 2004.
49. Ditl P, Rieger F. Designing suspension-mixing systems. *Chem Eng Progr*. 2006;102(1):22–30.
50. Zwietering TN. Suspending of solid particles in liquid by agitators. *Chem Eng Sci*. 1958;8:244–253.
51. Nienow AW. Suspension of solid particles in turbine agitated baffled vessels. *Chem Eng Sci*. 1968;23:1453–1459.
52. Armenante PM, Nagamine EU. Effect of low off-bottom impeller clearance on the minimum agitation speed for complete suspension of solids in stirred tanks. *Chem Eng Sci*. 1998;53:1757–1775.
53. Ayranci I, Kresta SM. Design rules for suspending concentrated mixtures of solids in stirred tanks. *Chem Eng Res Des*. 2011;89(10):1961–1971.
54. Özcan-Taskin G. The effect of impeller-to-tank diameter ratio on draw down of solids. *Chem Eng Sci*. 2003;58(10):2011–2022.
55. Bhattacharya S, Hebert D, Kresta S. Air Entrainment in Baffled Stirred Tanks. *Chem Eng Res Des*. 2007;85(5):654–664.
56. Bhattacharya S, Kresta S. Surface feed with minimum by-product formation for competitive reactions. *Chem Eng Res Des*. 2004;82(9):1153–1160.
57. Fournier MC, Falk L, Villermaux J. A new parallel competing reaction system for assessing micromixing efficiency: Experimental approach. *Chem Eng Sci*. 1996;51(23).
58. Guichardon P, Falk L. Characterisation of micromixing efficiency by the iodide-iodate reaction system. *Chem Eng Sci*. 2000;55:4233–4243.
59. Assirelli M, Bujalski W, Eaglesham A, Nienow AW. Intensifying micromixing in a semi-batch reactor using a Rushton turbine. *Chem Eng Sci*. 2005;60:2333–2339.
60. Nouri L, Legrand J, Benmalek N, Imerzoukene F, Yeddou A-R, Halet F. Characterisation and comparison of the micromixing efficiency in torus and batch stirred reactors. *Chem Eng J*. 2008;142(1):78–86.
61. Assirelli M, EJW Wynn, Bujalski W, Eaglesham A, Nienow AW. An extension to the incorporation model of micromixing and its use

in estimating local specific energy dissipation rates. *Ind Eng Chem Res*. 2008;47:3460–3469.
62. Siddiqui SW, Zhao Y, Kukukova A, Kresta SM. Characteristics of a confined impinging jet reactor: energy dissipation, homogeneous and heterogeneous reaction products, and effect of unequal flow. *Ind Eng Chem Res*. 2009;48(17):7945–7958.
63. Bourne JR. Comments on the iodide/iodate method for characterising micromixing. *Chem Eng J*. 2008;140(1–3):638–641.
64. Johnson BK, Prud'home RK. Chemical processing and micromixing in confined impinging jets. *AIChE J*. 2003;49(9):2264–2282.
65. Patterson GK, Paul EL, Kresta SM, Etchels AW. *Mixing and chemical reactions*. In: Paul EL, Atiemo-Obeng VA, Kresta SM, eds. *Handbook of Industrial Mixing: Science and Practice*. John Wiley & Sons, Inc.; 2004.
66. Reeder M, Benz G. Proper impeller systems ensure mixing performance. *Chem Process*. 1997:63–64.
67. Bezerra AC, Joaquim-Junior CF, Nunhez JR. Determining an optimal design and operational conditions for a commercial impeller using computational fluid dynamics (CFD). Paper presented at: AIChE Annual Meeting; 2003.
68. Armenante PM, Nagamine EU. Effect of low off-bottom impeller clearance on the minimum agitation speed for complete suspension of solids in stirred tanks. *Chem Eng Sci*. 1998;53(9):1757–1775.
69. Ayranci I, Machado MB, Derksen J, Nobes D, Kresta S. Effect of geometry on the mechanisms for off bottom solids suspension. Paper presented at: 22nd North American Mixing Forum; 2010; Victoria, BC, Canada,.
70. Ibrahim S, Nienow AW. Particle suspension in the turbulent regime: the effect of impeller type and impeller/vessel configuration. *Chem Eng Res Des*. 1996;74(6):679–688.
71. White AM, Brenner E, Phillips GA, Morrison MS. Studies in Agitation - IV. Power Measurements. V. The Correlation of Power Data. American Institute of Chemical Engineers – Transactions. 1934;30: 570–596.

Manuscript received Apr. 8, 2011, and revision received July 18, 2011.